

Article

Visible Light Driven Spherical CuBi_2O_4 with Surface Oxygen Vacancy Enhanced Photocatalytic Activity: Catalyst Fabrication, Performance, and Reaction Mechanism

Xin Zhong ^{1,2,*}, Yihong Cai ¹, Heping Bai ^{1,2}, Wei Huang ¹ and Binxue Zhou ¹

¹ Department of Environmental Engineering and Science, Beijing Normal University, Zhuhai 519000, China; wohehuli@sina.com (Y.C.); baiheping@bnu.edu.cn (H.B.); huangwei@bnu.edu.cn (W.H.); zbxbnuz@bnu.edu.cn (B.Z.)

² College of Education for the Future, Beijing Normal University at Zhuhai, Zhuhai 519000, China

* Correspondence: zhongxin@bnu.edu.cn; Tel.: +86-(0)-756-368-3012

Received: 21 July 2020; Accepted: 14 August 2020; Published: 17 August 2020



Abstract: Here, a spherical CuBi_2O_4 catalyst with surface oxygen vacancy was fabricated through a facile hydrothermal method, which exhibited remarkable enhanced photocatalytic activity of refractory chemicals in the heterogeneous sulfate radical-based Fenton-like reaction under visible light emitting diode (LED) light irradiation. The property of the catalysts was systematically characterized by scanning electron microscopy (SEM)/high resolution transmission electron microscopy (HRTEM), X-ray diffraction (XRD), X-ray photoelectron spectroscopy (XPS), and UV/vis methods. The effects of parameters of solution pH, potassium peroxymonosulfate (PMS) concentration, catalyst dosage, and catalyst reusability on Rhodamine B (RhB) degradation were investigated. In the interface reaction, the improved photodegradation efficiency could be attributed to the decomposition of PMS, which produced sulfate radicals and hydroxyl radicals owing to the transmission of photo-generated electron/hole pairs. Herein, the introduction of surface oxygen vacancy as well as the cycling of copper valence states (Cu(II)/Cu(I) pairs) can facilitate the production of free reactive radicals, leading to the high degradation efficiency. The catalyst showed high removal efficiency and presented good cycle stability in the reaction. Additionally, the free radical quencher experiment and electron spin resonance (EPR) experiments were conducted, and a proposed photocatalytic mechanism was also illustrated.

Keywords: CuBi_2O_4 ; visible LED light; peroxymonosulfate

1. Introduction

Owing to the rapid development of industry and fast growth of the population, the increased water pollution problem has attracted much more attention. To get the solution for these deteriorated water situations, it was really urgent to develop effective and economic technologies to eliminate these problems [1–3]. In recent years, advanced oxidation processes (AOPs) have brought more concern in the degradation of organic pollutants, which was considered really difficult to degrade by traditional methods [4–6]. Among these various AOPs, sulfate radical-based advanced oxidation processes (SR-based AOPs) possessed high removal efficiency of these concomitants, leading to the formation of sulfate radical (SO_4^-), which had similar redox potential with hydroxyl radicals [7–9]. Additionally, heterogeneous catalyst was employed for the activation of persulfate (PS) or potassium peroxymonosulfate (PMS, trade name Oxone) in SR-Fenton like oxidation process to achieve degradation and mineralization of contaminants in the wastewater. By introducing the visible light in the

heterogeneous SR-Fenton like system (i.e., heterogeneous SR-photo-Fenton like process), the reaction rate was improved in the reaction, which was also widely studied.

In the heterogeneous SR-photo-Fenton like process, the heterogeneous catalyst played a great role for the degradation efficiency. Firstly, the heterogeneous catalysts were effective for the PMS activation, leading to the decomposition of PMS and the formation of sulfate radicals [10–12]. On the other hand, the catalyst could also be stimulated by the visible light, while the generated hole/electron pairs could participate in the degradation process. Many kinds of heterogeneous catalysts have been investigated and applied in the heterogeneous SR-photo-Fenton like process, such as hybrid metal-organic framework (MIL53(Fe)) [13], inorganic oxide heterojunction ($\text{CuBi}_2\text{O}_4/\text{Bi}_2\text{O}_3$) [14], metal oxides (Co_3O_4) [15], and perovskite structure (BiFeO_3) [16]. In the heterogeneous SR-photo-Fenton like process, PMS was not only an oxidant, but also an electron acceptor, which could prevent the recombination of photo-generated holes and electrons [17–19]. The formed holes and electrons could react with PMS, facilitating the generation of sulfate radicals and hydroxyl radicals. Thus, it could improve the reduction between the high valence state and the low valence state of metal ions, facilitating the cycling of transition metal ions. It was considered that the synergistic effect existed between the catalyst/visible light process and heterogeneous SR-Fenton like reaction [20–23]. Unfortunately, the heterogeneous catalyst possessed high efficiency and stability was still rare, and the reaction mechanism needs further exploration in the heterogeneous SR-photo-Fenton like process.

In recent years, Bi-based catalysts, which acted as the photocatalyst for the degradation of contaminants owing to their unique properties and narrow band gap, have received more attention, facilitating the application of visible light. CuBi_2O_4 , as one of p-type Bi-based semiconductor, have aroused widespread concern as it took advantage of the low band gap (1.3–3.7 eV) and high stability [24–26]. The low band gap provided much convenience in the absorption of low energy photons and a better response to the visible light, which has shown notable photocatalytic performance in heterogeneous SR-Fenton like systems [27–29]. By the introduction of visible light, the degradation efficiency was enhanced owing to the reduction of transition Cu ions and photo-generated holes/electrons pairs on the surface of catalyst. Moreover, the photocatalytic performance by single usage of CuBi_2O_4 was unsatisfied, which suffered quick recombination of photogenerated holes and electrons. The degradation efficiency of the target pollutant was assumed to be further improved by using pure CuBi_2O_4 catalyst alone. On the other hand, to achieve better degradation efficiency, a large amount of photocatalyst was utilized in these systems. It was reported that, in the presence of PMS/PS, which acted as the electron acceptor, the photocatalytic activity was much improved, while the comparison between the absence and presence of PMS/PS by the application of Bi-based catalyst is listed in Table S1. Moreover, the photocatalysis performance of CuBi_2O_4 could also be improved by coupling with other semiconductors, such as $\text{Ag}_2\text{S}/\text{CQDs}$ [30], Bi_2MoO_6 [31], Ag_3PO_4 [32], and WO_3 [33]. On the other hand, the introduction of surface oxygen vacancies on catalyst was considered an effective way to improve its photocatalytic activity, which can grip the photo-generated holes and electrons and inhibit the recombination of the hole/electron pairs. Many studies investigated the good catalytic activity of catalyst with surface oxygen vacancies, such as $\text{Fe(III)}/\text{Bi}_2\text{MoO}_6$ [34], BiOBr [35], and TiO_2 [36]. With the presence of surface oxygen vacancy on the catalyst, the results proved that the band gap was narrowed and the separation and migration of photo-generated electron/holes was facilitated, resulting in better degradation efficiency.

In this study, CuBi_2O_4 with surface oxygen vacancy ($\text{CuBi}_2\text{O}_4\text{-OVs}$) was synthesized by the one-pot hydrothermal method, which was used in the heterogeneous SR-photo-Fenton like reaction for the removal of RhB. Visible LED light was chosen as the light source instead of the high-power xenon lamp or gold halide/tungsten lamp owing to its long working life, broad emission spectrum, and cost-effectiveness, and was considered as an efficient light source for removal of pollutants in wastewater. The cycling catalytic activity and copper ion leaching was carefully evaluated. The effects of initial pH, PMS concentration, and catalyst dosage were investigated. Therefore, on the basis of the various characterization analyses, a possible catalytic mechanism for the heterogeneous SR-photo-Fenton like

reaction by the usage of CuBi₂O₄-OVs catalyst was proposed. Radical quenching experiments and EPR tests were conducted to evaluate the main reactive free radicals. Overall, these results showed a novel strategy for the heterogeneous SR-photo-Fenton like reactions in wastewater treatment.

2. Results

2.1. Synthesis of Catalysts

A hydrothermal method was used to synthesize the CuBi₂O₄ catalyst with surface oxygen vacancy. Here, 2 mM Bi(NO₃)₃·5H₂O and 1 mM Cu(NO₃)₂·3H₂O were dissolved in 10 mL of ethylene glycol, respectively. Then, both solutions were mixed under stirring. Afterward, 30 mL ethanol and 0.3 g of glucose were added to the mixed solution. After being completely dissolved, the mixture was transferred into the 100 mL Teflon-lined stainless-steel autoclave and kept at 160 °C for 12 h. The solid was centrifuged and washed with deionized water and ethanol, which was dried at 70 °C for 24 h, which denoted as CuBi₂O₄-OVs. CuBi₂O₄ was also prepared without the addition of glucose. The glucose was used in the synthesis procedure, which played a great role on the morphology of the nanocomposites owing to the reduction effect, thus further improving the photocatalytic performance of the catalyst. Pure CuO and Bi₂O₃ were also prepared by the above method with the addition of Cu(NO₃)₂·3H₂O or Bi(NO₃)₃·5H₂O, respectively.

2.2. Material Characterization

X-ray diffraction (XRD) pattern was performed using a Bruker D8ADVANCE X-ray diffractometer with a graphite monochromatic Cu K α radiation ($\lambda = 1.54 \text{ \AA}$) at the accelerating voltage 40 kV and the current 30 mA over the 2θ scanning range of 10–80°. Scanning electron microscopy (SEM) was characterized on a Hitach SU8220 field emission with X-ray energy dispersive spectra (EDS) instrument, which would find out the element distribution. High resolution transmission electron microscopy (TEM) images were obtained using FEI Talos F200S with high-resolution at 200 kV. The X-ray photoelectron spectroscopy (XPS) was carried out on Thermo Fisher ESCALAB250Xi. The diffuse reflectance spectrum (DRS) was operated on ultraviolet visible near infrared spectrophotometer with Shimadzu UV-3600 Plus. The Brunauer-Emmett-Teller (BET) specific surface area, pore size, and volumes were analyzed by N₂ adsorption–desorption technology using automatic micromeritics instrument corporation TriStar II 3020.

2.3. Photocatalytic Performance Experiments

In the experimental setup, a 30 W LED lamp (30 W, 460 nm, Xujia Company, Shanghai, China) was employed as the light source. Further, 0.1 g photocatalyst was added to 200 mL of RhB solution (20 mg/L). Before the light turned on, the mixture was magnetically stirred in the dark for 60 min in order to obtain the absorption–desorption equilibrium. Then, 0.049 g PMS was added in the system and LED lights were turned on. The sample was taken out and filtered through 0.22 μm membrane filters; the concentrations of RhB and total organic carbon (TOC) were measured by UV/vis spectrophotometer (UV 3600 II, Shanghai, China) and TOC (Elementar vario) analyzer, respectively. Each sample was measured three times and the average values are shown in the figures. Electron spin resonance (ESR, JES FA200, JEOL) was used to measure the intensity of free radicals in methanol and deionized water. The copper leaching measurements were performed using the inductively coupled plasma mass spectrometry (ICP-MS) method (Agilent 7000). In the batch experiments, the degradation of RhB was fitted well with the pseudo first order kinetics model, which can be expressed as Equation (1).

$$\ln C/C_0 = -k_{\text{app}} \times t \quad (1)$$

where C refers to the concentration of RhB at time t , C_0 refers to the initial RhB concentration, k_{app} refers to the kinetic rate constant, and t refers to the reaction time.

3. Discussion

3.1. Characterization of Prepared Samples

The morphology and microstructure of the as-prepared CuBi_2O_4 and CuBi_2O_4 -OVs were characterized by SEM and HRTEM. Figure 1 presented that the CuBi_2O_4 sample was composed of a sphere-like morphology, which was made of nanocrystals of 20–40 nm thickness. However, it was also observed that large bulks were presented on the surface with agglomeration, owing to the anisotropic growth of crystals on the surface. The diameter of the sphere was in the width of ~400 nm. On the other hand, the morphology of CuBi_2O_4 -OVs synthesized after the addition of glucose showed smaller diameter of ~350 nm with a wool-ball like morphology, which was different with the CuBi_2O_4 . The results can be attributed to the reductant of glucose, which prevent the growth of crystallization, resulting in the decreased crystallinity of the CuBi_2O_4 sample. Furthermore, the elemental distribution of the CuBi_2O_4 -OVs composite was determined by energy dispersive spectroscopy (EDS). It was observed that there were three elements detected in the as-prepared samples, that is, Cu, Bi, and O, where the atomic ratio of Cu and Bi was close to 1:2.

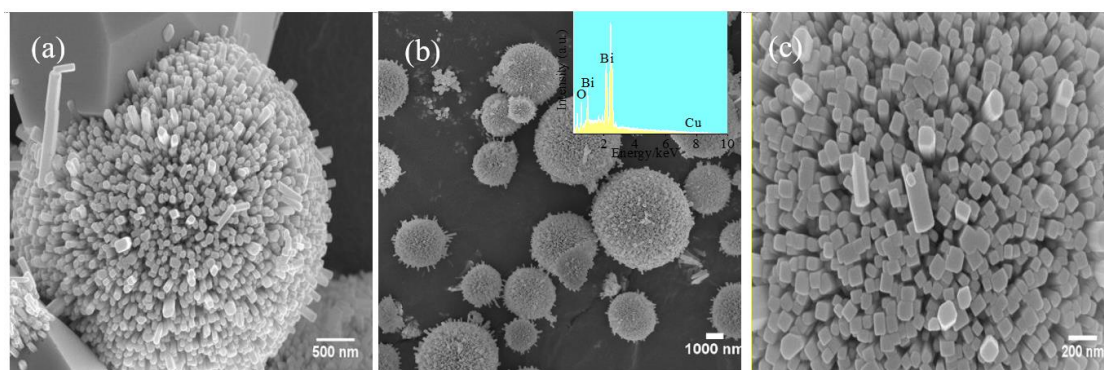


Figure 1. Scanning electron microscopy (SEM) images of as-prepared (a) CuBi_2O_4 and (b,c) CuBi_2O_4 -OVs; the inset is the energy dispersive spectroscopy (EDS) spectra of CuBi_2O_4 -OVs.

The HRTEM images clearly showed the lattice spacing of 0.245 nm and 0.253 nm, which was attributed to the (310) plane of the CuBi_2O_4 and CuBi_2O_4 -OVs samples, respectively, which was shown in Figure 2 [37]. Moreover, the EDS element mapping image of Cu, Bi, and O demonstrated the homogeneous distribution of these elements, which were presented on the surface of catalyst. However, the lattice edges of the CuBi_2O_4 -OVs sample were not distinct, found with disordered and blurred boundaries, which could be attributed to the introduction of surface oxygen vacancies. The TEM image of CuBi_2O_4 -OVs showed that the average size of the particles was close to 64 nm, where the particles presented partial agglomeration. The results of HRTEM images were consistent with the XRD data.

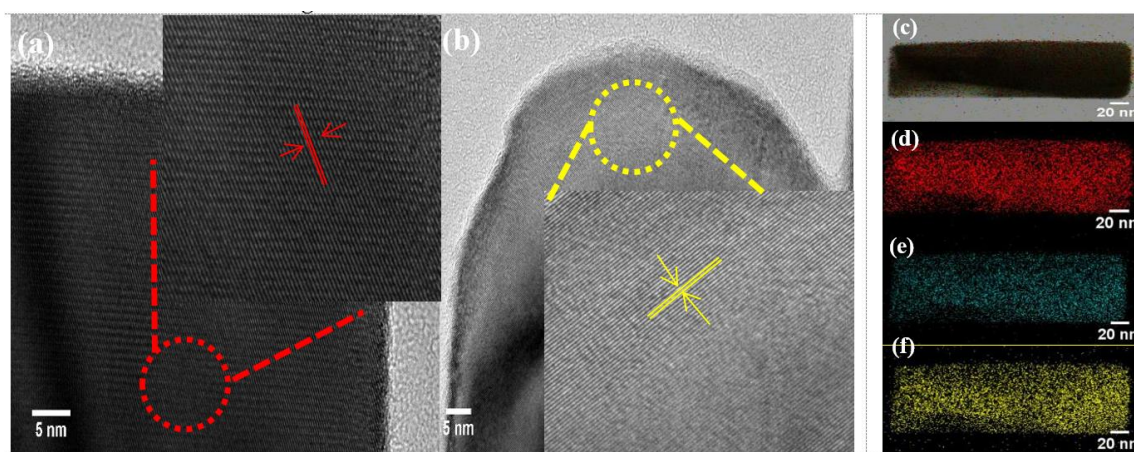


Figure 2. Transmission electron microscopy (TEM) images of as-prepared (a) CuBi_2O_4 and (b) CuBi_2O_4 -OVs, and (c) all elements EDS mapping images of CuBi_2O_4 -OVs, (d) Bi 4f, (e) Cu 2p, and (f) O 1s. The inset image is magnified image of the encircled area.

The crystal properties of the prepared CuBi_2O_4 -OVs, Bi_2O_3 , and CuO samples were characterized by XRD, which is shown in Figure 3. All the diffraction peaks of CuBi_2O_4 -OVs corresponded well to the phase of CuBi_2O_4 (JCPDS No. 48-1886). No impurities were found, indicating the preparation procedure was successful and the crystal structure of CuBi_2O_4 was unchanged during the synthesis [38,39]. The diffraction peaks were narrow and strong, which showed the good crystallization of the CuBi_2O_4 catalyst. With the introduction of surface oxygen vacancy, the intensity of diffraction peaks was slightly decreased. Diffraction peaks of CuO (JCPDS 44-0706) and Bi_2O_3 (JCPDS 27-0050) were also identified, demonstrating the pure crystal structure of synthesized catalysts. Moreover, the prepared samples possessed an average size of around 53.2 nm according to the Debye–Scherrer formula, which was in good agreement with SEM and TEM results.

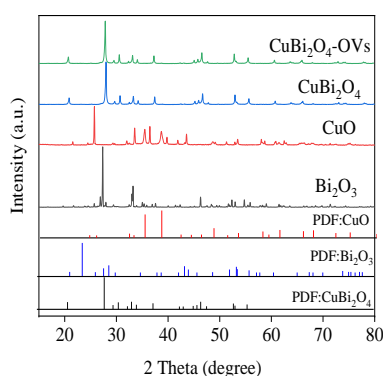


Figure 3. X-ray diffraction (XRD) patterns of as-prepared catalysts.

The chemical composition and element state of the prepared samples were carried out by the XPS method. As shown in Figure 4, the peaks of Bi, O, Cu, and trace C were found on the surface of as-prepared samples, which were sharp and clear. The characteristic peaks of Bi 4f were centered at 158.6 eV and 163.9 eV, corresponding to Bi 4f_{5/2} and Bi 4f_{7/2}, which indicated the existence of Bi³⁺ [40]. It was observed that the peaks were slightly shifted to higher binding energy owing to the introduction of surface oxygen vacancy. The peak observed at 955.5 eV with a satellite peak at 964.8 eV in the XPS spectra of Cu 2p was assigned to Cu 2p_{1/2}, and the peak of Cu 2p_{3/2} centered at 934.3 eV would be deconvoluted to 935.6 eV and 932.8 eV, respectively, which was considered as Cu(II) and reduced copper species [41]. The presence of reduced copper species on the surface of sample could be

attributed to the reduction of Cu(II), which facilitated the heterogeneous SR-photo-Fenton like reaction by the cycling reaction between Cu(II) and Cu(I). The peak centered around 530 eV can be denoted as O 1s, which shifted to a higher binding energy owing to the electron attraction effect of oxygen vacancy. The characteristic peak of O 1s could be deconvoluted into three internal peaks at 529.7 eV, 531.5 eV, and 532.5 eV in the fresh catalyst, representing the lattice oxygen, metal-O bonds (Bi-O, Cu-O), hydroxyl groups, and absorbed H₂O on the surface, respectively [42]. The peak of hydroxyl groups and absorbed H₂O in CuBi₂O₄-OVs took a much higher proportion than that of the CuBi₂O₄ samples. Additionally, the metal-O bonds were also different, which further proved the formation of surface oxygen vacancy on the catalyst. The proportion of the three peaks was changed after the heterogeneous SR-photo-Fenton like reaction, demonstrating the participation of the H₂O and oxygen vacancy in the reactions, leading to the formation of reactive oxygen radicals. The results also proved that there was a redox transition of Cu ions under LED light irradiation.

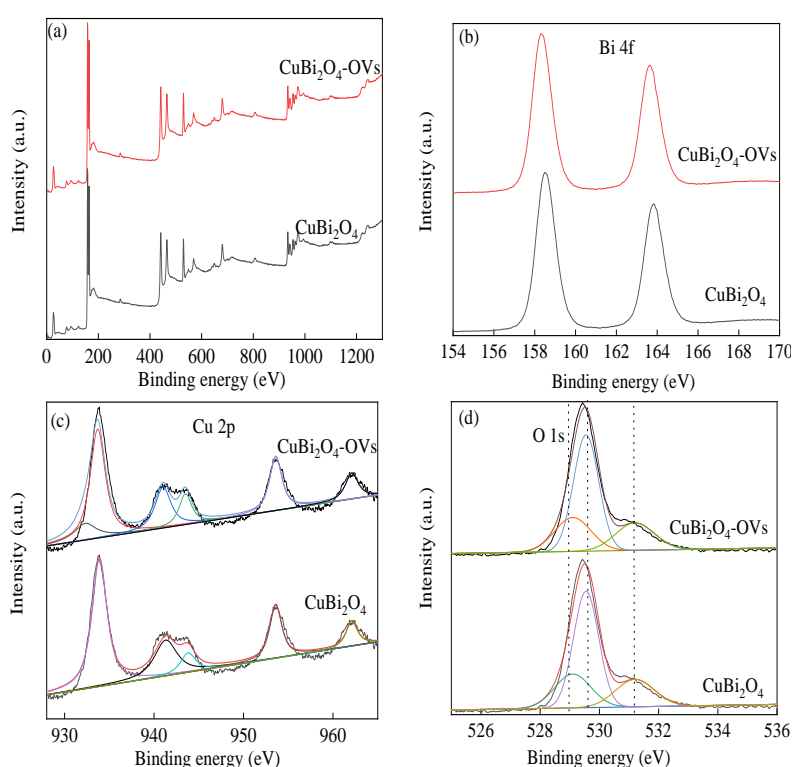


Figure 4. X-ray photoelectron spectroscopy (XPS) spectra of as-prepared catalysts. (a) full-scale XPS spectra, (b) Bi 4f, (c) Cu 2p, and (d) O 1s.

The UV/vis diffusion spectra of the CuBi₂O₄ and CuBi₂O₄-OVs catalyst were shown in Figure 5. It was observed that both the CuBi₂O₄ and CuBi₂O₄-OVs catalyst showed a long band absorption in the visible light region, implying good response to the visible light. However, the absorption area in the visible light region was higher in the CuBi₂O₄-OVs than in the CuBi₂O₄ catalyst owing to the introduction of surface oxygen vacancy. The results proved that the enhanced absorption in visible light region would result in better catalytic activity. The band gap energy (E_g) of CuBi₂O₄ and CuBi₂O₄-OVs was determined by the Tauc model, which is commonly used in the semiconductor catalyst [43].

$$ah\nu = A(h\nu - E_g)^{n/2} \quad (2)$$

where a , $h\nu$, A and E_g , are the absorbance, photon energy, a constant, and the band gap, respectively. The band gap energy of the CuBi₂O₄ and CuBi₂O₄-OVs catalyst was calculated to be fixed at 1.83 eV and 1.72 eV, respectively, which was assumed to perform good photocatalytic activity under visible

LED light irradiation. In the presence of surface oxygen vacancy, the narrowed band gap showed enhanced adsorption ability to visible light, promoting the separation of photo-generated holes and electrons pairs, causing the enhancement of photocatalytic activity. The N_2 absorption/desorption isotherms of the $CuBi_2O_4$ and $CuBi_2O_4$ -OVs catalyst are shown in Figure S1. The isotherms of both the $CuBi_2O_4$ and $CuBi_2O_4$ -OVs catalyst presented type H3 isotherms. The BET surface area of $CuBi_2O_4$ was $4.76\text{ m}^2/\text{g}$ and the pore size was around 10.9 nm , as the BET surface area of $CuBi_2O_4$ -OVs was $5.01\text{ m}^2/\text{g}$ and the pore size was 11.1 nm . With the presence of surface oxygen vacancy, the BET surface area and pore size was slightly increased, which is listed in Table S2.

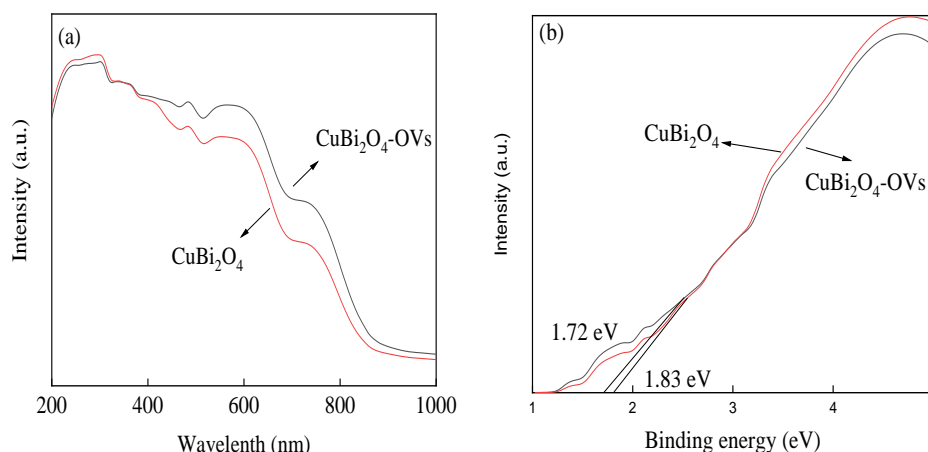


Figure 5. (a,b) UV/vis diffusion reflectance spectra of as-prepared catalysts.

3.2. Heterogeneous SR-Photo Degradation of RhB

The prepared catalysts have no adsorption removal efficiency on RhB in the reaction time owing to the limited BET surface area. Negligible removal of RhB was obtained by using PMS alone and using LED light alone, owing to hardly any production of reactive free radicals. Figure 6 shows the degradation efficiency of photocatalysis, heterogeneous SR-Fenton reaction, and heterogeneous SR-photo-Fenton like reaction was 29.4%, 56.8%, and 87.9%, respectively. The value of reaction constant k_{app} for heterogeneous SR-photo-Fenton like process was higher than the sum of photocatalysis and heterogeneous SR-Fenton like reaction, which demonstrated there was a synergistic effect for RhB degradation in heterogeneous SR-photo-Fenton like reaction with $CuBi_2O_4$ -OVs as catalyst. Herein, compared with the $CuBi_2O_4$ -OVs catalyst, the removal efficiency of RhB was 100% and 40.9% for CuO and Bi_2O_3 , respectively. On the other hand, with the introduction of surface oxygen vacancy, the synergistic effect between the heterogeneous SR-Fenton like reaction and photocatalysis could improve the degradation activity of RhB as well as the degradation rate constant [44]. The results might be attributed to the increased hydroxyl group on the surface, which formed more reactive oxygen species in the heterogeneous SR-photo-Fenton like reaction. The separation and transmission of photo-generated holes and electrons was also improved owing to the presence of surface oxygen vacancy, leading to better degradation efficiency. The addition of visible LED light to the heterogeneous SR-Fenton like systems enhanced the RhB removal degradation efficiency and rate constant. Consequently, the heterogeneous SR-photo-Fenton like system showed the highest removal efficiency for RhB by using $CuBi_2O_4$ -OVs catalyst combined with surface oxygen vacancy [45].

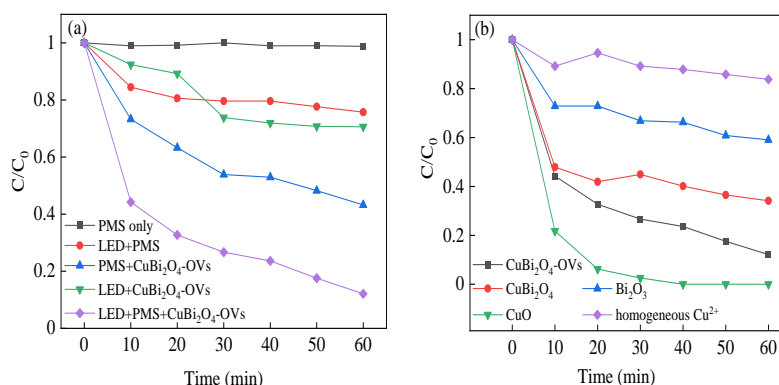


Figure 6. (a) Comparison of RhB degradation activity in different systems; (b) effect of different catalyst on RhB degradation. Reaction conditions: RhB (20 mg/L), PMS (0.4 mM), catalyst (0.5 g/L), neutral pH.

The pseudo-first-order kinetic model was applied to calculate the degradation rate constants, which fitted well with the results. The k_{app} values were 0.0064, 0.0126, and 0.0304 h⁻¹ for photocatalysis, heterogeneous SR-Fenton like reaction, and heterogeneous SR-photo-Fenton like reaction, respectively, which demonstrated the existence of a synergistic effect. Moreover, the metal leaching problem was very important in the heterogeneous reaction, which directly affected the stability of the heterogeneous catalyst. The leaching copper was very low and ranged from 0.020 to 0.0895 mg/L as the pH value declined from 10.7 to 3.2. The SR-photo-Fenton like reaction with 0.0895 mg/L copper ions in the system was also carried out and showed a poor contribution to PMS activation, evidencing that the catalyst played a significant role in the system. Therefore, photo-generated holes and electrons would participate in the redox transmission of copper ions in the heterogeneous SR-photo-Fenton like reaction, improving the formation of reactive oxygen species, leading to the enhancement of removal efficiency [46].

3.3. Effect of Reaction Conditions

Then, the reaction conditions were explored to get the best removal efficiency. As shown in Figure 7a, the removal efficiency of RhB declined from 86.2% to 37.9% as the solution pH climbed from 3.2 to 4.9. When the solution pH further climbed from 4.9 to 8.8, the degradation efficiency and rate constant were almost at the same level. Moreover, the removal efficiency of RhB was enhanced to 96.6% as the solution pH was raised to 10.7. In the acidic solution, the formation of SO₅²⁻ ions was obtained and showed no catalytic activity [47]. The results showed that PMS possessed more stability rather than decomposed to sulfate radicals, thus retarding the degradation efficiency in highly acidic conditions [48]. When the solution pH came to neutral and basic condition, the hydroxyl radicals formed, which showed similar redox potential with sulfate radicals, resulting in better RhB removal efficiency. The removal rate remained unchanged in the pH range of 4.9–8.8, which proved that the CuBi₂O₄-OVs catalyst would be effective in a wide range of pH in the heterogeneous SR-photo-Fenton like process.

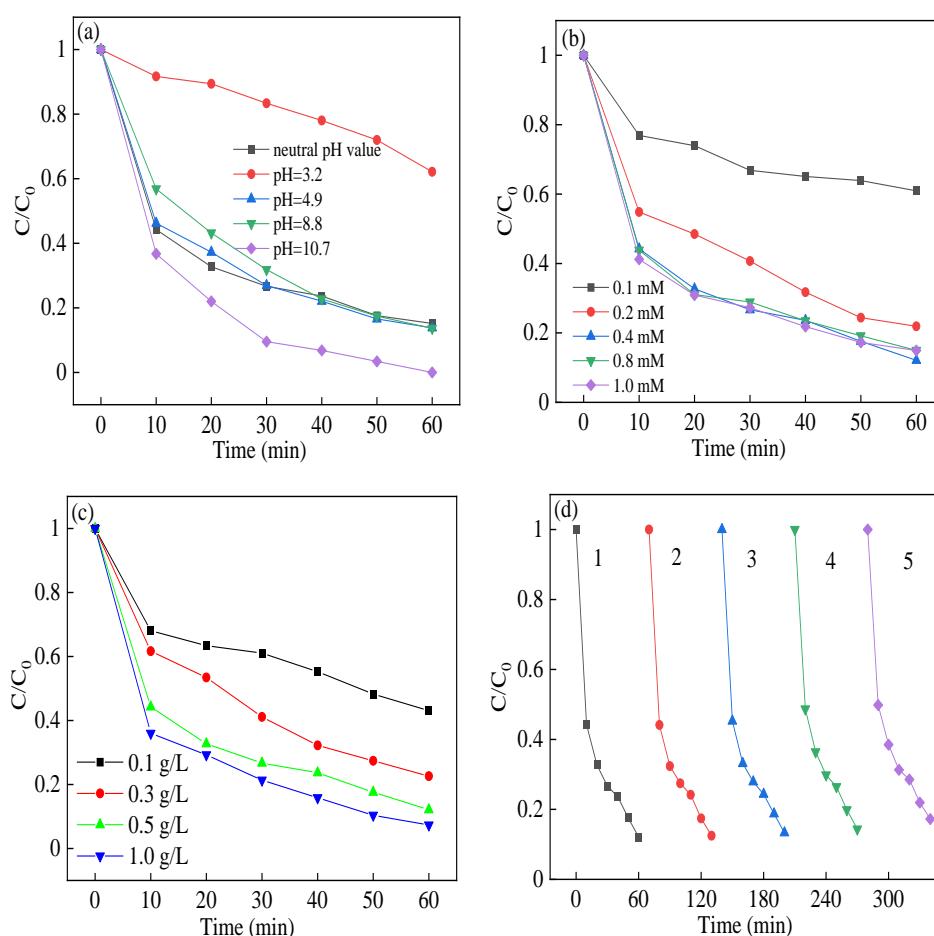


Figure 7. Effect of (a) reaction initial pH value; (b) PMS concentration; (c) catalyst dosage; and (d) reuse on RhB degradation in heterogeneous sulfate radical (SR)-photo-Fenton like reaction. Reaction conditions: RhB (20 mg/L), PMS (0.1–1.0 mM), catalyst (0.1–1.0 g/L), pH in the range of 3.2–10.7 in (a–c); PMS (0.4 mM), catalyst (0.5 g/L), neutral pH in (d).



The removal efficiency of RhB with different PMS concentrations in the range of 0.1–1.0 mM in the heterogeneous SR-photo-Fenton like reaction was shown in Figure 7b. The degradation efficiency of RhB increased from 39.1% to 87.9% with the increased PMS concentration, and the degradation rate constant varied from 0.0071 to 0.0304 h^{-1} . However, the degradation efficiency of RhB was not further increased; as the PMS concentration rose higher than 0.4 mM, the rate constant remained nearly unchanged. The results could be attributed to the reactive sites on the surface of catalyst, which participated in the activation of PMS, leading to greater generation of oxidant species in the increment of PMS concentrations; on the other hand, overdosed oxidants will compete with other reactive radicals, resulting in the consumption of free radicals and declined removal efficiency of RhB [49]. When the PMS concentration was too high, it would inhibit the reaction between the reactive species and the contaminants, resulting in the decreased removal rate constant, which was a waste of PMS.

The removal efficiency of RhB in heterogeneous SR-photo-Fenton like reaction with different catalyst dosages was shown in Figure 7c. When the catalyst dosage increased from 0.1 g/L to 1.0 g/L, the removal efficiency climbed from 57.1% to 92.7% in the reaction time, where the degradation rate

changed from 0.012 to 0.0391 h^{-1} . As the catalyst dosage was over 0.5 g/L, the increasing rate of k_{app} was not fast enough when the catalyst dosage was fixed at 1.0 g/L. Firstly, with the increment of the catalyst addition, more reactive sites were employed to generate more reactive oxygen species, where more surface area was provided in the reaction. Secondly, the excessive catalyst would be an obstacle to the adsorption and transmission of visible light [50]. This phenomenon would give a negative effect on the excitation of electrons and lead to the reduction of activation efficiency. All the above results indicated that the prepared $\text{CuBi}_2\text{O}_4\text{-OVs}$ catalyst showed high and effective activity for RhB removal in the heterogeneous SR-photo-Fenton like reaction.

The recycling experiments of $\text{CuBi}_2\text{O}_4\text{-OVs}$ were evaluated under the optimized reaction conditions, which are shown in Figure 7d. The RhB degradation efficiency remained high in five successive reactions, and only showed slightly decreased efficiency in the fifth cycling experiment with 82.7% RhB removal. This might be attributed to the occupancy of reactive sites on the surface of catalyst in the successive reactions, where the leaching copper also affected the removal efficiency. Moreover, the rate constant also remained in the range of 0.0304 to 0.0258 h^{-1} . The leached copper element was no more than 0.0895 mg/L, demonstrating the stability of synthesized $\text{CuBi}_2\text{O}_4\text{-OVs}$ in heterogeneous SR-photo-Fenton like reaction. Compared with the fresh composite, the XRD diffraction peaks of $\text{CuBi}_2\text{O}_4\text{-OVs}$ had no obvious change after the reaction, which are shown in Figure S2. The major phase of the $\text{CuBi}_2\text{O}_4\text{-OVs}$ catalyst showed no obvious difference between the fresh and used catalyst, indicating the stability of the $\text{CuBi}_2\text{O}_4\text{-OVs}$ structure. The XPS peak of O 1s in the used catalyst showed slightly increased owing to the increment of oxygen or the water adsorption on the surface of catalyst. All the above results showed the catalyst had good reusability and stability in the heterogeneous SR-photo-Fenton like reaction.

TOC experiments were also used to evaluate the mineralization of RhB under optimal reaction conditions, which were shown in Figure 8. The TOC degradation was 13.3%, 32.8%, and 63.2% in the photocatalysis reaction, heterogeneous SR-Fenton like reaction, and heterogeneous SR-photo-Fenton like reaction, respectively. The results showed the mineralization of RhB was satisfied owing to the synergism effect, and were in good agreement with the degradation efficiency of RhB. Moreover, the $\text{CuBi}_2\text{O}_4\text{-OVs}$ was also employed for the removal of other organic contaminants in the heterogeneous SR-photo-Fenton reaction, such as Orange II, methyl red (MR), ciprofloxacin (CIP), and levofloxacin (LVF). The degradation efficiency of Orange II and MR was 85.1% and 83.7% in the reaction time, whereas the degradation of CIP and LVF was about 10.4% and 16.2%, respectively. The results showed that the heterogeneous SR-photo-Fenton like reaction was effective for mostly common organic pollutants, especially for the removal of dyes.

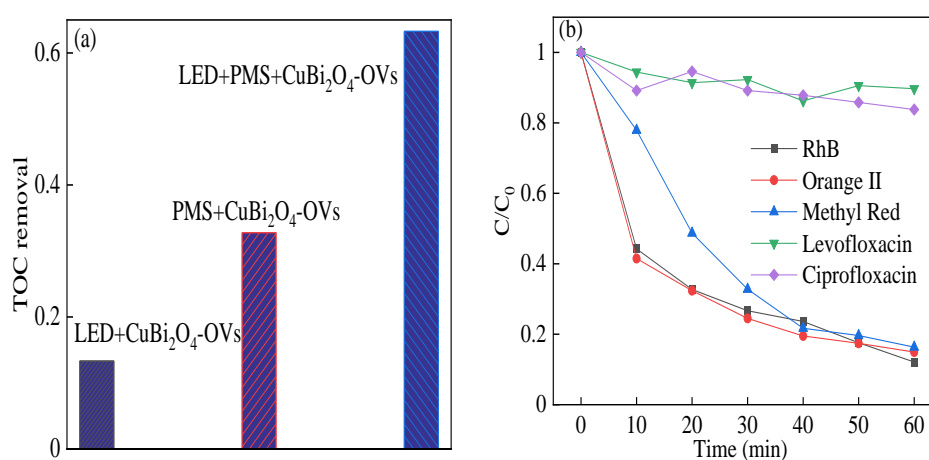


Figure 8. (a) Total organic carbon (TOC) removal of RhB; (b) degradation of various contaminants in heterogeneous SR-photo-Fenton like reaction. Reaction conditions: contaminants (20 mg/L), PMS (0.4 mM), catalyst (0.5 g/L), neutral pH.

3.4. Reaction Mechanism

It was known that the reactive radical species dominated the reaction rate and efficiency in the heterogeneous SR-photo-Fenton like reaction. In order to identify the reactive radicals, radical quencher chemicals were applied in the system to find the possible free radicals. Compared with the reaction with sulfate radicals, the reaction between tert-Butyl alcohol (TBA) and hydroxyl radicals was really fast. In this case, TBA was usually considered as the trapping agent of $\cdot\text{OH}$. Methanol (MeOH) could react with sulfate and hydroxyl radicals in the meantime, which was used as the trapping agent for sulfate radicals and hydroxyl radicals. It can be seen in Figure 9a that the degradation efficiency of RhB was 79.5% and 70.6%, which slightly decreased in the presence of TBA and MeOH compared with the control experiment. Herein, it was proposed that both sulfate radicals and hydroxyl radicals were formed in the reaction. However, the two free radicals took a little contribution for the reaction, implying the two scavenging chemicals took a moderate inhibition in the reaction. Moreover, in order to identify the existence of photogenerated holes and superoxide radicals, p-benzoquinone (BQ) and sodium oxalate (SO, $\text{Na}_2\text{C}_2\text{O}_4$) were used as quenching chemicals for the reactive species. When BQ and SO chemicals were added in the solution, the degradation efficiency of RhB was declined to 15.8% and 40.2%, which demonstrated the superoxide radicals and holes were also generated and dominated in the reaction. It was assumed that the superoxide, photogenerated holes, sulfate radicals, and hydroxyl radicals were all produced in the reaction. The sulfate radicals, holes, and superoxide radicals played a dominant role in the RhB removal process, leading to enhancement of the photocatalytic reaction.

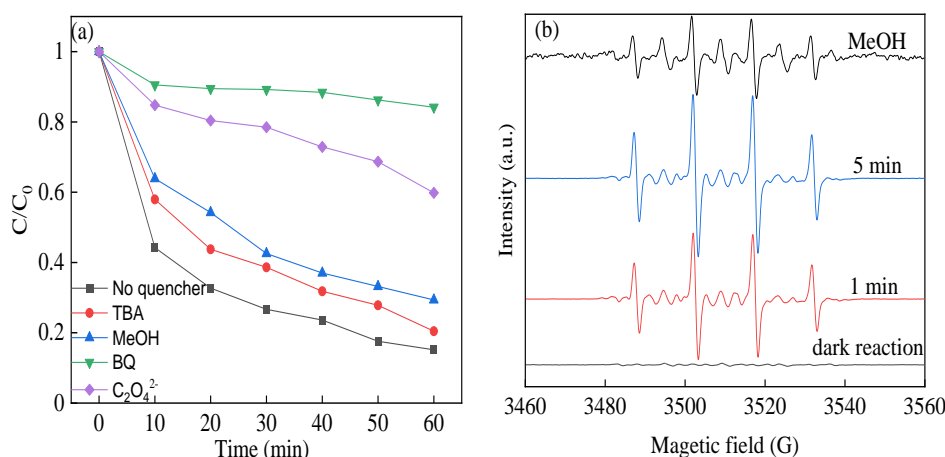


Figure 9. (a) Different quenching chemicals to remove RhB; (b) DMPO spin-trapping EPR spectra in heterogeneous SR-photo-Fenton like reaction. BQ, p-benzoquinone.

In order to evidence the existence of free reactive radicals, EPR experiments were also conducted using 5, 5-Dimethyl-1-Pyrrolidine-N-oxide (DMPO) as a spin trapping agent, as shown in Figure 9b. Weak typical peaks of DMPO-OH were identified under dark condition, indicating certain number of radicals were produced as a result of the activation of PMS. However, when the heterogeneous SR-Fenton like system was irradiated by visible LED light, strong signals of DMPO-OH peaks were observed. The EPR signals of DMPO- SO_4 were found with weak intensity owing to the quick reaction with H_2O , leading to the generation of hydroxyl radicals, which made it difficult to capture the signal in the solution [51]. The signal remained sharp after 5 min reaction, evidencing the persistent production of these free radicals. Moreover, the signal of DMPO- O_2 radicals was also observed, which proved the presence of superoxide radicals in the systems. Thus, the CuBi_2O_4 -OVs catalyst could produce lots of free reactive radicals in the heterogeneous SR-photo-Fenton like reaction, which agreed well with the results of the quenching experiments.

3.5. Proposed Reaction Mechanism

Figure 10 illustrates the mechanism in the heterogeneous SR-photo-Fenton like reaction using the $\text{CuBi}_2\text{O}_4\text{-OVs}$ catalyst under LED light irradiation on the basis of the above results. In the XPS spectra, the peaks for Cu element could be attributed to Cu(II) and Cu(I). The redox pair of Cu(I)/Cu(II) could participate in the decomposition of PMS to generate $\text{SO}_4^{\cdot-}$ and $\cdot\text{OH}$, which was much higher after the reaction than that of fresh catalyst. The continuous redox of Cu(II) occurred through the reduction caused by generated electrons, leading to the production of reduced Cu species. Meanwhile, the electrons could jump from CB to VB on the catalyst surface, which was occupied with rich surface oxygen vacancy, facilitating the rapid conversion of Cu(II)/Cu(I) pairs. With the presence of surface oxygen vacancy, the free radicals were formed more quickly, leading to better degradation efficiency. Moreover, surface oxygen vacancy could be considered as a defect on the catalyst surface, acting as the reactive sites, which was effective to prevent the recombination of photo-generated holes/electrons, leading to better catalytic activity [52]. Additionally, the visible region of catalyst was also extended, which was helpful for the visible light adsorption on the surface.

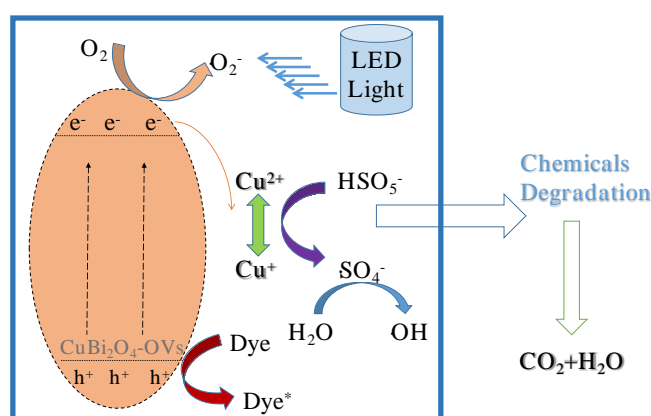
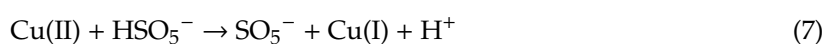
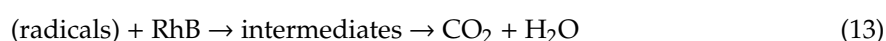
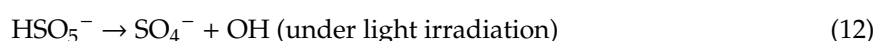


Figure 10. Mechanism of heterogeneous SR-photo-Fenton like degradation of RhB using the $\text{CuBi}_2\text{O}_4\text{-OVs}$ catalyst.

In conclusion, as the $\text{CuBi}_2\text{O}_4\text{-OVs}$ catalyst was irradiated by visible LED light, the production of photo-generated hole and electrons occurred, which would react with PMS to generate free radicals. PMS was applied as the electron acceptor and the oxidant in the heterogeneous SR-photo-Fenton like reaction, which suppressed the recombination of holes and electrons, leading to better degradation efficiency [53]. As the surface oxygen vacancy was presented on the surface of catalyst, the free radicals were quickly formed owing to the quick transmission of photo-generated carriers and good separation efficiency of the pairs. The extended response to the visible light would also be attributed to the introduction of surface oxygen vacancy. Then, with the persistent attack of superoxide, holes, sulfate radicals, and hydroxyl radicals, the target pollutant RhB was gradually degraded in the reaction and mineralized to CO_2 and H_2O .





4. Conclusions

In this study, the CuBi₂O₄-OVs catalyst was prepared and applied in a heterogeneous SR-photo-Fenton like system. The removal of RhB fitted well with the pseudo first-order kinetics model. The optimal experiment condition was obtained such that the catalyst dosage was fixed at 0.5 g/L and PMS concentration was fixed at 0.4 mM under neutral pH, which showed a synergism effect of the photocatalysis and heterogeneous SR-Fenton like reaction. The introduction of surface oxygen vacancy could prevent the recombination of photogenerated holes and electrons and narrow the band gap of CuBi₂O₄, leading to higher degradation efficiency. With the increased dosage of PMS and catalyst, the removal efficiency was improved, but retarded with overdosed addition owing to side competitive reactions. The CuBi₂O₄-OVs catalyst exhibited good photocatalytic performance. Moreover, the reusability of catalyst was excellent in five successive experiments with low leaching of Cu ions. The roles of superoxide radicals, holes, sulfate radicals, and hydroxyl radicals were identified by quencher chemicals and EPR experiments. The reaction mechanism was also proposed in the heterogeneous SR-photo-Fenton like reaction. Therefore, the heterogeneous SR-photo-Fenton like system has good aspect for the treatment of organic pollutant in wastewater.

Supplementary Materials: The following are available online at <http://www.mdpi.com/2073-4344/10/8/945/s1>, Figure S1: N₂ adsorption–desorption isotherm of CuBi₂O₄ and CuBi₂O₄-OVs; Figure S2: XRD patterns of the CuBi₂O₄-OVs catalyst before and after the reaction; Table S1: Studies on of Bi-based catalysts in the photocatalytic reactions; Table S2: Surface area, pore volume, pore size of CuBi₂O₄, and CuBi₂O₄-OVs samples.

Author Contributions: Methodology, X.Z.; investigation, Y.C., H.B., and X.Z.; resources, W.H. and B.Z.; writing—original draft preparation, X.Z.; writing—review and editing, X.Z.; project administration, X.Z., W.H., and B.Z. All authors have read and agreed to the published version of the manuscript.

Funding: This work is financially supported by the Project of Youth Innovative Foundation of Guangdong Province of China (Grant No. 201912017QX); Provincial undergraduate innovation and Entrepreneurship Project (S202013177014); Promotion Project Funds of Beijing Normal University, Zhuhai (Grant No. 201850001); Quality Engineering Project of Beijing Normal University, Zhuhai (Grant No. 201832); and Plan of Youth Teachers of Guangdong Higher Education Association (Grant No. 19GYB060).

Acknowledgments: This work is financially supported by Project of Youth Innovative Foundation of Guangdong Province of China for help in XRD, SEM, TEM, and XPS analysis.

Conflicts of Interest: The authors declare that there is no conflict of interests.

References

1. Frank, S.N.; Bard, A.J. Heterogeneous photocatalytic oxidation of cyanide and sulfite in aqueous solutions at semiconductor powders. *J. Phys. Chem.* **1977**, *81*, 1484–1488. [[CrossRef](#)]
2. Li, R.; Li, T.; Zhou, Q. Impact of titanium Dioxide (TiO₂) modification on its application to pollution treatment—A Review. *Catalyst* **2020**, *10*, 804. [[CrossRef](#)]

3. Karthikeyan, C.; Arunachalam, P.; Ramachandran, K.; Al-Mayouf, A.M.; Karuppuchamy, S. Recent advances in semiconductor metal oxides with enhanced methods for solar photocatalytic applications. *J. Alloy. Compd.* **2020**, *828*, 15. [[CrossRef](#)]
4. Gray, H.E.; Powell, T.; Choi, S.; Smith, D.S.; Parker, W.J. Organic phosphorus removal using an integrated advanced oxidation-ultrafiltration process. *Water Res.* **2020**, *1821*, 115968.
5. Gonzalez, T.; Dominguez, J.R.; Correia, S. Neonicotinoids removal by associated binary, tertiary and quaternary advanced oxidation processes: Synergistic effects, kinetics and mineralization. *J. Environ. Manag.* **2020**, *2611*, 110156. [[CrossRef](#)]
6. Wang, J.; Zhuan, R. Degradation of antibiotics by advanced oxidation processes: An overview. *Sci. Total Environ.* **2020**, *701*, 135023. [[CrossRef](#)]
7. Zhao, Q.; Mao, Q.; Zhou, Y.; Wei, J.; Liu, X.; Yang, J.; Luo, L.; Zhang, J.; Chen, H.; Chen, H.; et al. Metal-free carbon materials-catalyzed sulfate radical-based advanced oxidation processes: A review on heterogeneous catalysts and applications. *Chemosphere* **2017**, *189*, 224–238. [[CrossRef](#)]
8. Oh, W.D.; Dong, Z.; Lim, T.T. Generation of sulfate radical through heterogeneous catalysis for organic contaminants removal: Current development, challenges and prospects. *Appl. Catal. B* **2016**, *1945*, 169–201. [[CrossRef](#)]
9. Hu, P.; Long, M. Cobalt-catalyzed sulfate radical-based advanced oxidation: A review on heterogeneous catalysts and applications. *Appl. Catal. B* **2016**, *181*, 103–117. [[CrossRef](#)]
10. Shukla, P.; Sun, H.; Wang, S.; Ang, H.M.; Tade, M.O. Co-SBA-15 for heterogeneous oxidation of phenol with sulfate radical for wastewater treatment. *Catal. Today* **2011**, *175*, 380–385. [[CrossRef](#)]
11. Wang, Y.; Indrawirawan, S.; Duan, X.; Sun, H.; Ang, H.M.; Tade, M.O.; Wang, S. New insights into heterogeneous generation and evolution processes of sulfate radicals for phenol degradation over one-dimensional α -MnO₂ nanostructures. *Chem. Eng. J.* **2015**, *266*, 12–20. [[CrossRef](#)]
12. Wu, C.H.; Yang, M.T.; Lin, K.Y.A. Magnetic Co/Fe nanohybrid supported on carbonaceous marcosphere as a heterogeneous catalyst for sulfate radical-based chemical oxidation. *J. Environ. Chem. Eng.* **2018**, *6*, 426–434. [[CrossRef](#)]
13. Zhang, Y.; Zhou, J.; Chen, J.; Feng, X.; Cai, W. Rapid degradation of tetracycline hydrochloride by heterogeneous photocatalysis coupling persulfate oxidation with MIL-53(Fe) under visible light irradiation. *J. Hazard. Mater.* **2020**, *392*, 122315. [[CrossRef](#)] [[PubMed](#)]
14. Wang, Y.; Liu, C.; Zhang, Y.; Meng, W.; Yu, B.; Pu, S.; Yuan, D.; Qi, F.; Xu, B.; Chu, W. Sulfate radical-based photo-Fenton reaction derived by CuBi₂O₄ and its composites with α -Bi₂O₃ under visible light irradiation: Catalyst fabrication, performance and reaction mechanism. *Appl. Catal. B* **2018**, *235*, 264–273. [[CrossRef](#)]
15. Lv, C.; Liang, H.; Chen, H.; Wu, L. Hydroxyapatite supported Co₃O₄ catalyst for enhanced degradation of organic contaminants in aqueous solution: Synergistic visible-light photo-catalysis and sulfate radical oxidation process. *Microchem. J.* **2019**, *149*, 103959. [[CrossRef](#)]
16. Soltani, T.; Lee, B.K. Enhanced formation of sulfate radicals by metal-doped BiFeO₃ under visible light for improving photo-Fenton catalytic degradation of 2-chlorophenol. *Chem. Eng. J.* **2017**, *313*, 1258–1268. [[CrossRef](#)]
17. Zhang, M.W.; Lin, K.Y.A.; Huang, C.F.; Tong, S. Enhanced degradation of toxic azo dye, amaranth, in water using Oxone catalyzed by MIL-101-NH₂ under visible light irradiation. *Sep. Purif. Tech.* **2019**, *227*, 115632. [[CrossRef](#)]
18. Karbasi, M.; Karimzadeh, F.; Raeissi, K.; Giannakis, S.; Pulgarin, C. Improving visible light photocatalytic inactivation of E. coli by inducing highly efficient radical pathways through peroxymonosulfate activation using 3-D, surface-enhanced, reduced graphene oxide (rGO) aerogels. *Chem. Eng. J.* **2020**, *396*, 125189. [[CrossRef](#)]
19. Bi, W.; Wu, Y.; Dong, W. The degradation of oxytetracycline with low concentration of persulfate sodium motivated by copper sulphate under simulated solar light. *Chem. Eng. J.* **2020**, *393*, 122782. [[CrossRef](#)]
20. Wang, A.; Chen, Z.; Zheng, Z.; Xu, H.; Yan, K. Remarkably enhanced sulfate radical-based photo-Fenton-like degradation of levofloxacin using the reduced mesoporous MnO@MnO_x microspheres. *Chem. Eng. J.* **2020**, *379*, 122340. [[CrossRef](#)]
21. Feng, Q.; Zhou, J.; Luo, W.; Ding, L.; Cai, W. Photo-Fenton removal of tetracycline hydrochloride using LaFeO₃ as a persulfate activator under visible light. *Ecotoxicol. Environ. Saf.* **2020**, *198*, 110661. [[CrossRef](#)] [[PubMed](#)]

22. Chen, Q.; Ji, F.; Guo, Q.; Fan, J.; Xu, X. Combination of heterogeneous Fenton-like reaction and photocatalysis using Co-TiO₂ nanocatalyst for activation of KHSO₅ with visible light irradiation at ambient conditions. *J. Environ. Sci.* **2014**, *26*, 2440–2450. [[CrossRef](#)] [[PubMed](#)]
23. Zhu, B.; Cheng, H.; Ma, J.; Qin, Y.; Kong, Y.; Komarneni, S. Bi₂MoO₆ microspheres for the degradation of orange II by heterogeneous activation of persulfate under visible light. *Mater. Lett.* **2020**, *261*, 127099. [[CrossRef](#)]
24. Li, M.; Tian, X.; Zou, X.; Han, X.; Du, C.; Shan, B. Promoting photoelectrochemical hydrogen evolution activity of CuBi₂O₄ photocathode through ramping rate control. *Int. J. Hydrogen Energy* **2020**, *45*, 15121–15128. [[CrossRef](#)]
25. Ma, C.; Ma, D.K.; Yu, W.; Chen, W.; Huang, S. Ag and N-doped graphene quantum dots co-modified CuBi₂O₄ submicron rod photocathodes with enhanced photoelectrochemical activity. *Appl. Surf. Sci.* **2019**, *481*, 661–668. [[CrossRef](#)]
26. Chen, X.; Dai, Y.; Guo, J. Hydrothermal synthesis of well-distributed spherical CuBi₂O₄ with enhanced photocatalytic activity under visible light irradiation. *Mater. Lett.* **2015**, *161*, 251–254. [[CrossRef](#)]
27. Sabri, M.; Habibi-Yangjeh, A.; Ghosh, S. Novel ZnO/CuBi₂O₄ heterostructures for persulfate-assisted photocatalytic degradation of dye contaminants under visible light. *J. Photoch. Photobiol. A* **2020**, *391*, 112397. [[CrossRef](#)]
28. Zhang, H.; Nengzi, L.; Li, X.; Wang, Z.; Cheng, X. Construction of CuBi₂O₄/MnO₂ composite as Z-scheme photoactivator of peroxydisulfate for degradation of antibiotics. *Chem. Eng. J.* **2020**, *386*, 124011. [[CrossRef](#)]
29. Oh, W.D.; Dong, Z.; Lim, T.T. Hierarchically-structured Co-CuBi₂O₄ and Cu-CuBi₂O₄ for sulfanilamide removal via peroxydisulfate activation. *Catal. Today* **2017**, *280*, 2–7. [[CrossRef](#)]
30. Gao, H.; Wang, F.; Wang, S.; Wang, X.; Yi, Z.; Yang, H. Photocatalytic activity tuning in a novel Ag₂S/CQDs/CuBi₂O₄ composite: Synthesis and photocatalytic mechanism. *Mater. Res. Bull.* **2019**, *115*, 140–149. [[CrossRef](#)]
31. Shi, W.; Li, M.; Huang, X.; Ren, H.; Guo, F.; Tang, Y.; Lu, C. Construction of CuBi₂O₄/Bi₂MoO₆ p-n heterojunction with nanosheets-on-microrods structure for improved photocatalytic activity towards broad-spectrum antibiotics degradation. *Chem. Eng. J.* **2020**, *394*, 125009. [[CrossRef](#)]
32. Chen, X.; Yu, C.; Zhu, R.; Li, N.; Chen, M.; Lin, Q.; Xu, S.; Chen, X.; Wang, H. Photocatalytic performance and mechanism of Z-Scheme CuBi₂O₄/Ag₃PO₄ in the degradation of diclofenac sodium under visible light irradiation: Effects of pH, H₂O₂, and S₂O₈²⁻. *Sci. Total Environ.* **2020**, *711*, 134643. [[CrossRef](#)]
33. Wang, L.; Huang, T.; Yang, G.; Lu, C.; Dong, F.; Li, Y.; Guan, W. The precursor-guided hydrothermal synthesis of CuBi₂O₄/WO₃ heterostructure with enhanced photoactivity under simulated solar light irradiation and mechanism insight. *J. Hazard. Mater.* **2020**, *381*, 120956. [[CrossRef](#)]
34. Fu, F.; Shen, H.; Sun, X.; Xue, W.; Shoneye, A.; Ma, J.; Luo, L.; Wang, D.; Wang, J.; Tang, J. Synergistic effect of surface oxygen vacancies and interfacial charge transfer on Fe(III)/Bi₂MoO₆ for efficient photocatalysis. *Appl. Catal. B* **2019**, *247*, 150–162. [[CrossRef](#)]
35. Lyu, J.; Hu, Z.; Li, Z.; Ge, M. Removal of tetracycline by BiOBr microspheres with oxygen vacancies: Combination of adsorption and photocatalysis. *J. Phys. Chem. Solids* **2019**, *129*, 61–70. [[CrossRef](#)]
36. Li, D.; Haneda, H.; Labhsetwar, N.K.; Hishita, S.; Ohashi, N. Visible-light-driven photocatalysis on fluorine-doped TiO₂ powders by the creation of surface oxygen vacancies. *Chem. Phys. Lett.* **2005**, *401*, 579–584. [[CrossRef](#)]
37. Xie, Y.; Zhang, Y.; Yang, G.; Liu, C.; Wang, J. Hydrothermal synthesis of CuBi₂O₄ nanosheets and their photocatalytic behavior under visible light irradiation. *Mater. Lett.* **2013**, *107*, 291–294. [[CrossRef](#)]
38. Shan, W.; Hu, Y.; Bai, Z.; Zheng, M.; Wei, C. In situ preparation of g-C₃N₄/bismuth-based oxide nanocomposites with enhanced photocatalytic activity. *Appl. Catal. B* **2016**, *188*, 1–12. [[CrossRef](#)]
39. Hossain, M.K.; Samu, G.F.; Gandha, K.; Santhanagopalan, S.; Liu, J.P.; Janaky, C.; Rajeshwar, K. Solution combustion synthesis, characterization, and photocatalytic activity of CuBi₂O₄ and its nanocomposites with CuO and α-Bi₂O₃. *J. Phys. Chem. C* **2017**, *121*, 8252–8261. [[CrossRef](#)]
40. Brezesinski, K.; Ostermann, R.; Hartmann, P.; Perlich, J.; Brezesinski, T. Exceptional Photocatalytic Activity of Ordered Mesoporous β-Bi₂O₃ Thin Films and Electrospun Nanofiber Mats. *Chem. Mater.* **2010**, *22*, 3079–3085. [[CrossRef](#)]

41. Zhang, L.; Lyu, L.; Nie, Y.; Hu, C. Cu-doped Bi₂O₃/Bi⁰ composite as an efficient Fenton-like catalyst for degradation of 2-chlorophenol. *Sep. Purif. Tech.* **2016**, *157*, 203–208. [[CrossRef](#)]
42. Zhang, Y.; Liu, C.; Xu, B.; Qi, F.; Chu, W. Degradation of benzotriazole by a novel Fenton-like reaction with mesoporous Cu/MnO₂: Combination of adsorption and catalysis oxidation. *Appl. Catal. B* **2016**, *199*, 447–457. [[CrossRef](#)]
43. Zhang, X.; Wang, X.; Chai, J.; Xue, S.; Wang, R.; Jiang, L.; Wang, J.; Zhang, Z.; Dionysiou, D.D. Construction of novel symmetric double Z-scheme BiFeO₃/CuBi₂O₄/BaTiO₃ photocatalyst with enhanced solar-light-driven photocatalytic performance for degradation of norfloxacin. *Appl. Catal. B* **2020**, *272*, 119017. [[CrossRef](#)]
44. Sun, Q.; Wu, S.; Li, K.; Han, B.; Chen, Y.; Pang, B.; Yu, L.; Dong, L. The favourable synergistic operation of photocatalysis and catalytic oxygen reduction reaction by a novel heterogeneous CoFe₂O₄-TiO₂ nanocomposite. *Appl. Surf. Sci.* **2020**, *516*, 146142. [[CrossRef](#)]
45. Hu, J.; Li, J.; Cui, J.; An, W.; Liu, L.; Liang, Y.; Cui, W. Surface oxygen vacancies enriched FeOOH/Bi₂MoO₆ photocatalysis-fenton synergy degradation of organic pollutants. *J. Hazard. Mater.* **2020**, *384*, 121399. [[CrossRef](#)] [[PubMed](#)]
46. Chen, X.; Zhou, J.; Zhang, T.; Ding, L. Enhanced degradation of tetracycline hydrochloride using photocatalysis and sulfate radical-based oxidation processes by Co/BiVO₄ composites. *J. Water Process. Eng.* **2019**, *32*, 100918. [[CrossRef](#)]
47. Huang, J.; Zhang, H. Mn-based catalysts for sulfate radical-based advanced oxidation processes: A review. *Environ. Int.* **2019**, *133*, 105141. [[CrossRef](#)]
48. Chen, Z.; Bi, S.; Zhao, G.; Chen, Y.; Hu, Y. Enhanced degradation of triclosan by cobalt manganese spinel-type oxide activated peroxymonosulfate oxidation process via sulfate radicals and singlet oxygen: Mechanisms and intermediates identification. *Sci. Total Environ.* **2020**, *711*, 134715. [[CrossRef](#)]
49. Hao, S.M.; Yu, M.Y.; Zhang, Y.J.; Abdelkrim, Y.; Qu, J. Hierarchical mesoporous cobalt silicate architectures as high-performance sulfate-radical-based advanced oxidization catalysts. *J. Colloid. Interf. Sci.* **2019**, *545*, 128–137. [[CrossRef](#)]
50. Baran, N.Y.; Baran, T.; Mentş, A. Design of highly robust halloysite nanoclay supported palladium complex as a highly active heterogeneous catalyst for construction of biaryls. *Appl. Clay Sci.* **2019**, *18115*, 105225. [[CrossRef](#)]
51. Hu, L.; Wang, P.; Shen, T.; Wang, Q.; Zhang, G. The application of microwaves in sulfate radical-based advanced oxidation processes for environmental remediation: A review. *Sci. Total. Environ.* **2020**, *722*, 137831. [[CrossRef](#)] [[PubMed](#)]
52. You, J.; Sun, W.; Su, S.; Ao, Z.; Liu, C.; Yao, G.; Lai, B. Degradation of bisphenol A by peroxymonosulfate activated with oxygen vacancy modified nano-NiO-ZnO composite oxides: A typical surface-bound radical system. *Chem. Eng. J.* **2020**, *400*, 125915. [[CrossRef](#)]
53. Huang, Z.; Wu, P.; Liu, J.; Yang, S.; Chen, M.; Li, Y.; Niu, W.; Ye, Q. Defect-rich carbon based bimetallic oxides with abundant oxygen vacancies as highly active catalysts for enhanced 4-aminobenzoic acid ethyl ester (ABEE) degradation toward peroxymonosulfate activation. *Chem. Eng. J.* **2020**, *395*, 124936. [[CrossRef](#)]

